Eur. Phys. J. B **53**, 537–549 (2006)
DOI: 10.1140/epjb/e2006-00408-2

THE EUROPEAN PHYSICAL JOURNAL B

Theoretical imaging of current profiles in two-dimensional devices

A. Cresti[1,a], G. Grosso[2], and G. Pastori Parravicini[3]

[1] NEST-INFM, Scuola Normale Superiore, Piazza dei Cavalieri 7, 56126 Pisa, Italy
and
Dipartimento di Fisica 'E. Fermi', Università di Pisa, Largo B. Pontecorvo 3, 56127 Pisa, Italy
[2] NEST-INFM and Dipartimento di Fisica 'E. Fermi', Università di Pisa, Largo B. Pontecorvo 3, 56127 Pisa, Italy
[3] NEST-INFM and Dipartimento di Fisica 'A. Volta', Università di Pavia, via A. Bassi 6, 27100 Pavia, Italy

Received 7 April 2006 / Received in final form 29 September 2006
Published online 17 November 2006 –

Abstract. This paper addresses in a concise and rigorous way the basic tools for the study of local longitudinal and transverse microscopic currents in two-dimensional devices. The emphasis is on the optimized use of the Keldysh nonequilibrium Green's function theory together with the tight-binding representation of the electronic system. We elaborate general analytic expressions of current profiles, useful for modeling and simulating the local site-to-site flow of carriers; furthermore, in broken time-reversal symmetry, the formalism discerns unambiguously persistent and transport contributions to the bond currents. Our approach achieves a workable theoretical imaging, resolved in space and energy, of the microscopic currents through mesoscopic devices.

PACS. 72.10.Bg General formulation of transport theory – 73.63.-b Electronic transport in nanoscale materials and structures

1 Introduction

Space and energy resolved imaging of currents is fundamental for understanding electron transport in mesoscopic conductors. In fact, advances in experimental techniques based on scanning probe microscopy aimed to image coherent electron flow [1–5], but more generally the wide field of conductance (I/V) spectroscopy on nanodevices [6–8], has evidenced the importance of theoretical tools able not only to describe $I-V$ characteristics, but also to predict currents distributions for specific shapes of the device and external bias conditions.

A wide and well assessed literature exists on the calculation of ballistic transport in quantum devices and multilayer structures. Most of the methods adopted address the evaluation of the total current in the device, in the linear response regime and (almost) equilibrium conditions, expressing the conductance in terms of transmission probabilities in the scattering Landauer-Büttiker approach [9]. The presence of magnetic fields has further contributed to enrich the interest in analytic expressions for the evaluation of the conductance [10]. Among the different theoretical techniques developed for the evaluation of the microscopic currents, we mention transfer matrix methods [11], direct matching of the propagation modes in the leads with the wavefunctions of the scattering region [12,13], the density matrix approach [14] and the Green's function approach [15,16].

In particular, the nonequilibrium Green's function (NEGF) formalism, introduced by Kadanoff and Baym [17] and Keldysh [18] has emerged as a very successful tool [15,16,19,20] for its ability to handle systems regardless how near or how far from equilibrium they are driven. Moreover, when coupled with the Poisson equation, it is well suited for the self consistent determination of the potential profile in the device [21]. For ballistic transport in noninteracting electron systems, the NEGF formalism reproduces the Landauer theory of transport. In addition, a noticeable bonus of the formalism is that self-consistent nonequilibrium Dyson equations of the theory are given in terms of self-energies calculated by standard many-body diagrammatic techniques [22,23]. Thus, at least in principle, electron-electron [24–27] coupling, electron-phonon [28–32] interactions, alloy scattering [33], time-dependent interactions [34] can be included in the formalism at the desired (or reasonable) order of accuracy.

Even if the largest number of papers has focused on the evaluation of the total current through the lead-device-lead system, attempts have also been made to deduce expressions for the local spatial distribution of currents. This has generally been performed in the framework of the Landauer-Büttiker formalism by appropriate discretization of electronic wavefunctions [35] or by suitable projection operators into the atomic sites of the device, in

[a] e-mail: cresti@df.unipi.it

the tight-binding formalism [36]. Also the Wigner function approach to the NEGF formalism has been elaborated to investigate theoretically and numerically the electron density and current density in two-dimensional systems in the linear response regime [37].

The aim of this paper is to provide closed analytic expressions for the spatial distribution and energy resolution of the currents flowing through realistic devices, under finite external bias and also in the presence of magnetic fields. Our results are obtained by means of the Keldysh nonequilibrium Green's function appropriately inserted in the tight-binding formalism for the description of the device and the leads, and exploit recursive techniques [8,38] for the reduction of the huge number of degrees of freedom encountered in the description of open mesoscopic devices. A one-body picture of the electronic Hamiltonian is employed throughout this paper.

We start mapping the total system into a suitable discretized square lattice quantum wire, that mimics the actual mesoscopic sample under investigation. We then describe the site-to-site current in terms of the lesser Green's function obtained from the kinetic equations of the Keldysh theory. By means of appropriate manipulations of the generalized Dyson equations, the microscopic currents are finally expressed in terms of the retarded and advanced Green's functions, the retarded and advanced self-energies, and the Fermi distribution functions at finite temperatures of the leads.

In our procedure the real-space renormalization-recursive method [38–44] is found particularly convenient in the solution of the quantum kinetic equations both in the absence and in the presence of magnetic fields. In particular, in the presence of magnetic fields and broken time-reversal symmetry, we provide here exact analytic expressions for the transport and persistent contributions to the site-to-site currents, both longitudinal and transverse to the device. The determination of these contributions is unambiguous and their physical meaning is highlighted. We have also shown analytically that the longitudinal and transverse currents, flowing through a chosen column of the device, can be obtained from the knowledge of Green's function elements involving only the sites of the selected column; this makes the final expressions much appealing for numerical implementations and greatly limits the computational effort. In general it is thus possible at any chosen energy to describe the spatial distribution of the currents and their nature.

In previous work [39] we have shown the potentialities of the tight-binding Keldysh approach for the theoretical investigation of the current distributions in a random quantum wire in the transport regime of universal conductance fluctuations, in the study of the effect of a scanning tip on a two-dimensional electron gas, and in the analysis of scattering of edge currents through quantum point contacts [40]. In this paper we present a more complete deduction of the expressions used therein, and introduce analytic elaborations to give them the most economical form for the systematic modeling and simulation of devices.

In Section 2 the two-dimensional system under study and some basic definitions are introduced. The expressions for the longitudinal and transverse currents are deduced in Section 3; their simplification in the presence of time-reversal symmetry is reported in Section 4. In Section 5 we focus on the mathematical expressions elaborated for transport and persistent currents in broken time-reversal symmetry. Physical aspects behind the formalism are here illustrated by numerical simulations of the currents in quantum wires. In Section 6, the expression of current imaging at finite temperatures is reported. Section 7 contains the conclusions.

2 General considerations on the electronic current in two-dimensional devices

We start considering a two-dimensional device, whose electronic structure is described within the one-electron approximation in the tight-binding framework. For simplicity we confine our investigation to the case of a single orbital per site and nearest-neighbor interactions; whenever necessary the inclusion of multiorbitals per site, successive neighbor interactions, spin-orbit or spin-dependent terms, etc., can be dealt with similar procedures. A further advantage of the tight-binding description is its simplicity and accuracy to account for the effects of perpendicular magnetic fields [8] by means of appropriate Peierls phase factors in the site-to-site hopping parameters. The system under attention is schematically indicated in Figure 1.

It is convenient to partition the complete structure into two semi-infinite leads and a central device. In our case the device includes $M \times N$ sites, with coordinates ma, na and $m = 1, 2, \ldots, M$ and $n = 1, 2, \ldots, N$. The one-body electron Hamiltonian of the whole structure is initially separated into the unperturbed part, corresponding to the three regions of the device isolated one from the others, and the perturbation that couples them. We write

$$H = H_0 + W_{pert} \tag{1a}$$

where

$$H_0 = H_0^{(\text{left})} + H_0^{(\text{center})} + H_0^{(\text{right})} \tag{1b}$$

is the Hamiltonian of the three parts of the device not yet in interaction, and W_{pert} represents the perturbation. The various terms of the Hamiltonian can be written as follows (n runs over the N chains composing the system, m and m' run over the leads and device columns)

$$H_0^{(\text{left})} = \sum_{mn} E_{mn} c_{mn}^\dagger c_{mn} + \sum_{mn \neq m'n'} t_{mn,m'n'} c_{mn}^\dagger c_{m'n'}$$
$$(m, m' = 0, -1, -2, \ldots)$$
$$H_0^{(\text{center})} = \sum_{mn} E_{mn} c_{mn}^\dagger c_{mn} + \sum_{mn \neq m'n'} t_{mn,m'n'} c_{mn}^\dagger c_{m'n'}$$
$$(m, m' = 1,\ 2, \ldots,\ M)$$
$$H_0^{(\text{right})} = \sum_{mn} E_{mn} c_{mn}^\dagger c_{mn} + \sum_{mn \neq m'n'} t_{mn,m'n'} c_{mn}^\dagger c_{m'n'}$$
$$(m, m' = M+1, M+2, \ldots)$$

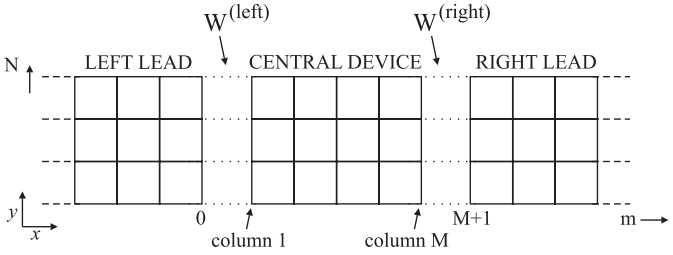

Fig. 1. Typical arrangement of a two-dimensional device for the analysis of current distribution.

where $c^{\dagger}_{mn}$ and c_{mn} denote creation and annihilation operators corresponding to the electronic orbital ϕ_{mn}. The perturbation is given by

$$W_{pert} = W^{(\mathrm{left})}_{pert} + W^{(\mathrm{right})}_{pert} \tag{2a}$$

where

$$W^{(\mathrm{left})}_{pert} = \sum_n t_{0n,1n} c^{\dagger}_{0n} c_{1n} + \sum_n t_{1n,0n} c^{\dagger}_{1n} c_{0n} \tag{2b}$$

$$W^{(\mathrm{right})}_{pert} = \sum_n t_{Mn,M+1\,n} c^{\dagger}_{Mn} c_{M+1\,n} + \sum_n t_{M+1\,n,Mn} c^{\dagger}_{M+1\,n} c_{Mn}. \tag{2c}$$

The "central device" is here embraced between Col. 1 and Col. M, as shown in Figure 1. The two semi-infinite regions on either side of the central device are in contact with particle reservoirs. The Fermi-Dirac distribution functions of the left and right reservoirs are denoted by $f_L(E)$ and $f_R(E)$ and the corresponding chemical potentials by μ_L and μ_R, respectively. The Green's functions of the structure with disconnected leads are denoted by $g^R, g^A, g^<, g^>$ (the superscripts stand for retarded, advanced, lesser and greater). With $G^R, G^A, G^<, G^>$ we denote the Green's functions of the complete system in the nonequilibrium steady state.

For the Green's function of the central device the following general relation holds [7,28]

$$G^R - G^A = -iG^R[\Gamma^{(\mathrm{left})} + \Gamma^{(\mathrm{right})}]G^A \tag{3}$$

where the matrix $\Gamma^{(\mathrm{left})}$ represents the coupling of Col. 1 to the part of the device on its left side, and the matrix $\Gamma^{(\mathrm{right})}$ represents the coupling of the Mth column to the part of the device on its right side; these two matrices are given by

$$\Gamma^{(\mathrm{left})}_{1n,1n'} = i\,\Sigma^{R(\mathrm{left})}_{1n,1n'} - i\,\Sigma^{A(\mathrm{left})}_{1n,1n'}$$

and

$$\Gamma^{(\mathrm{right})}_{Mn,Mn'} = i\,\Sigma^{R(\mathrm{right})}_{Mn,Mn'} - i\,\Sigma^{A(\mathrm{right})}_{Mn,Mn'},$$

where the self-energy operators on the border columns

$$\Sigma^{R,A(\mathrm{left})}_{1n,1n'} = t_{1n,0n} g^{R,A}_{0n,0n'} t_{0n',1n'}$$

$$\Sigma^{R,A(\mathrm{right})}_{Mn,Mn'} = t_{Mn,M+1\,n} g^{R,A}_{M+1\,n,M+1\,n'} t_{M+1\,n',Mn'}$$

describe the effects of the open leads on the retarded and advanced electron propagators in the central region of interest.

Before passing to proper elaborations of the above expressions, we specify some notations of frequent use in the following of this work. In general the matrix elements of a Green's function operator (say the retarded operator G^R) carry four lower labels $G^R_{mn,m'n'}(E)$: this is required to specify the propagator from the site $m'n'$ to the site mn. The abridged notation $G^R_{mm'}(E)$ is used to denote the propagator from a site (not yet specified) of column m' to a site (not yet specified) of column m. Thus $G^R_{mm'}(E)$ denotes a matrix of rank N, whose elements are

$$\left[G^R_{mm'}\right]_{nn'} = G^R_{mn,m'n'} = \langle \phi_{mn} | G^R | \phi_{m'n'} \rangle.$$

Equation (3) specified to the sites of Col. 1, takes the form

$$G^R_{11} - G^A_{11} = -iG^R_{11}\Gamma^{(\mathrm{left})}_{11} G^A_{11} - iG^R_{1M}\Gamma^{(\mathrm{right})}_{MM} G^A_{M1}, \tag{4a}$$

an identity exploited in the following.

Another important identity can be obtained by choosing as central region of the same system considered above the part which extends from column 1 to column M' ($M' \geq 1; M' \neq M$). In this case, replacing M with M' in equation (4a) we obtain the new relation

$$G^R_{11} - G^A_{11} = -iG^R_{11}\Gamma^{(\mathrm{left})}_{11} G^A_{11} - iG^R_{1M'}\Gamma^{(\mathrm{right})}_{M'M'} G^A_{M'1}. \tag{4b}$$

From equations (4a) and (4b) it follows

$$G^R_{1M'}\Gamma^{(\mathrm{right})}_{M'M'} G^A_{M'1} = G^R_{1M}\Gamma^{(\mathrm{right})}_{MM} G^A_{M1} \qquad (M, M' \geq 1)$$

which allows us to choose as "central device" the most convenient part of the complete system for calculations. In particular, setting $M' = 1$, we have the equality

$$G^R_{11}\Gamma^{(\mathrm{right})}_{11} G^A_{11} = G^R_{1M}\Gamma^{(\mathrm{right})}_{MM} G^A_{M1} \quad \text{for any} \quad M \geq 1. \tag{4c}$$

In the calculations of the currents a key ingredient is the quantity $G^R_{1M}\Gamma^{(\mathrm{right})}_{MM} G^A_{M1}$; by virtue of equation (4c), we can replace it by $G^R_{11}\Gamma^{(\mathrm{right})}_{11} G^A_{11}$. Thus for the calculation of currents in the two-terminal geometry under attention it is not needed the knowledge of the "inter-column" matrices of the type $G^{R,A}_{I,M}$ ($I \neq M$), but it is sufficient to consider the "intra-column" Green's functions $G^{R,A}_{I,I}$, with evident advantages in the numerical simulations. The identities summarized by equations (4) are by-products of the basic relationship (3), which in turn is embodied in the Keldysh kinetic equation for the lesser Green's function, discussed in the next section. In essence, these identities are the exact analytic expressions of the current conservation through any section of the system in steady nonequilibrium conditions.

After these introductory remarks, we pass now to the determination of the microscopic currents through the mesoscopic system.

3 Branch currents in a two-dimensional device

In Figure 1 the whole device has been (arbitrarily) split into three parts conventionally referred to as: "left lead" (Col. 0 and whatever is at its left), "central part" (whatever is at and within Col. 1 and Col. $M \geq 1$), "right lead" (Col. $M+1$ and whatever is at its right). In this section we elaborate the expressions for the energy-resolved and spatially-resolved microscopic currents that flow between the sites of Col. 0 and the adjacent sites of Col. 1 (longitudinal currents) and across the strand of sites of Col. 1 (transverse currents). The current profiles of the mesoscopic systems are then provided by scanning the "conceptual cut" throughout the region of interest of the devices under investigation.

3.1 Expression of the longitudinal currents

The longitudinal current flowing along the bond from site $0n$ to site $1n$ in steady state conditions is given by the expression [16]

$$I_{0n,1n} = \frac{2(-e)}{\hbar}\int \frac{dE}{2\pi}\, 2\Re\left[t_{0n,1n}G^{<}_{1n,0n}\right] = -i_0\int dE\, 2\Re\left[t_{0n,1n}G^{<}_{1n,0n}\right], \quad (5)$$

where $i_0 \equiv 2e/h = 7.748092\times 10^{-5}$ A/eV is the natural unit of spectral current; the factor 2 in i_0 takes account of spin degeneracy. (A convenient unit to express current is $I_0 = i_0 \times 1$ meV $= 77.48092$ nA.)

In equation (5) the matrix elements of the nonequilibrium Green's function $G^<$ involve an orbital in the left lead and an orbital in the central device. The first step in the elaboration of equation (5) is to deal with Green's function matrix elements $G^{R,A,<}$, which involve only orbitals on the central device region. To achieve this purpose one can use the general expression [8,18]

$$G^< = g^< + G^R\ W_{pert}\ g^< + G^<\ W_{pert}\ g^A \quad (6)$$

where Green's functions expressed by lower cases refer to the system, initially split into three uncoupled parts at time $t = -\infty$. From equations (6) and (2), we have the matrix elements

$$G^<_{1n,0n} = \sum_{n'} G^R_{1n,1n'}\, t_{1n',0n'}\, g^<_{0n',0n} + \sum_{n'} G^<_{1n,1n'}\, t_{1n',0n'}\, g^A_{0n',0n}.$$

The quantity in square brackets in the integrand in equation (5) becomes

$$\begin{aligned} t_{0n,1n}G^<_{1n,0n} &= \sum_{n'}\big[\, G^R_{1n,1n'}\, t_{1n',0n'}\, g^<_{0n',0n}t_{0n,1n} \\ &\qquad + G^<_{1n,1n'}\, t_{1n',0n'}\, g^A_{0n',0n}t_{0n,1n}\,\big] \\ &= \sum_{n'} G^R_{1n,1n'}\Sigma^{<(\mathrm{left})}_{1n',1n} + \sum_{n'} G^<_{1n,1n'}\Sigma^{A(\mathrm{left})}_{1n',1n} \\ &= \left[G^R_{11}\,\Sigma^{<(\mathrm{left})}_{11} + G^<_{11}\,\Sigma^{A(\mathrm{left})}_{11}\right]_{nn} \end{aligned}$$

where the lesser and advanced self-energy matrices are

$$\Sigma^{<(\mathrm{left})}_{1n',1n} = t_{1n',0n'}g^<_{0n',0n}t_{0n,1n}$$
$$\Sigma^{A(\mathrm{left})}_{1n',1n} = t_{1n',0n'}g^A_{0n',0n}t_{0n,1n}.$$

The expression (5) for the current is then

$$I_{0n,1n} = -i_0\int dE\, 2\Re\left[G^R_{11}\Sigma^{<(\mathrm{left})}_{11} + G^<_{11}\Sigma^{A(\mathrm{left})}_{11}\right]_{nn}. \quad (7)$$

To proceed further we need the expression of the lesser Green's function projected on the central device. This kinetic equation, which takes into account the injection or extraction of carriers from the leads to the central device, reads

$$\begin{aligned} G^< &= G^R\Sigma^{<(leads)}G^A \\ &= if_L G^R\Gamma^{(\mathrm{left})}G^A + if_R G^R\Gamma^{(\mathrm{right})}G^A, \end{aligned} \quad (8)$$

where all the matrices representing the operators are restricted to the basis orbitals belonging to the central device. In particular, using equation (8), we have for the lesser Green's function on the Col. 1 the following expression

$$G^<_{11} = if_L G^R_{11}\Gamma^{(\mathrm{left})}_{11}G^A_{11} + if_R G^R_{1M}\Gamma^{(\mathrm{right})}_{MM}G^A_{M1}. \quad (9)$$

Notice that equation (8) is valid regardless how near or how far the device is driven out of equilibrium. Suppose now, as a particular case, that the two leads (in the past remote) were kept in contact with two reservoirs having the same Fermi-Dirac distribution function f_0, so that $f_L = f_R \equiv f_0$. In this case, the central device is driven to the thermal equilibrium, with the lesser Green's function $G^< = -f_0(G^R - G^A)$. Inserting this expression into the first member of equation (8), and setting $f_L = f_R = f_0$ into the second member of equation (8), leads to equation (3). Thus relation (3) is a necessary ingredient to give sense to the kinetic equation (Eq. (8)).

Inserting into equation (7) the expression for the lesser Green's function, and the expression for the lesser self-energy of the left lead, one obtains

$$I_{0n,1n} = i_0\int dE\, 2\Re\left[f_L G^R_{11}\Sigma^{R(\mathrm{left})}_{11} - f_L G^R_{11}\Sigma^{A(\mathrm{left})}_{11} - if_L G^R_{11}\Gamma^{(\mathrm{left})}_{11}G^A_{11}\Sigma^{A(\mathrm{left})}_{11} - if_R G^R_{1M}\Gamma^{(\mathrm{right})}_{MM}G^A_{M1}\Sigma^{A(\mathrm{left})}_{11}\right]_{nn}. \quad (10a)$$

The above expression can also be written in the equivalent form

$$I_{0n,1n} = \int i_{0n,1n}(E)\, dE \tag{10b}$$

where the spectral current (or the current per unit energy) $i_{0n,1n}(E)$, is the integrand of the expression (10a) including the natural unit of spectral current i_0.

Equations (10a) and (10b) elaborated so far for the local current are exact and hold at any arbitrary temperature. For sake of simplicity, and without loss of generality, we now consider the expressions for current profiles at zero temperature. In fact, as outlined in Section 6, the treatment of current profiles at finite temperatures is trivial, and just follows step-by-step the treatment at zero temperature we are going to work out in this Section. At the absolute zero temperature, the two Fermi distribution functions become step functions $f_L(E) = \Theta(\mu_L - E)$ and $f_R(E) = \Theta(\mu_R - E)$; the spectral current, i.e. the integrand of equation (10a), then becomes

$$\begin{aligned} i_{0n,1n}(E) = i_0\, \Theta(\mu_L - E)\, 2\Re \Big[& G^R_{11} \Sigma^{R(\text{left})}_{11} - G^R_{11} \Sigma^{A(\text{left})}_{11} \\ & - i G^R_{11} \Gamma^{(\text{left})}_{11} G^A_{11} \Sigma^{A(\text{left})}_{11} \Big]_{nn} \\ + i_0\, \Theta(\mu_R - E)\, 2\Re & \Big[- i G^R_{1M} \Gamma^{(\text{left})}_{MM} G^A_{M1} \Sigma^{A(\text{left})}_{11} \Big]_{nn} . \end{aligned} \tag{11}$$

It is convenient to write down separately equation (11) in the case $\mu_L < \mu_R$ [hereafter referred to as case (a)] and in the case $\mu_R < \mu_L$ [hereafter referred to as case (b)]. The physical reason for this distinction is that carriers are injected from the right lead to the left lead in the former case, while in the latter case the opposite occurs; we can here anticipate that, in the presence of magnetic fields, the spatial distribution of currents (and hence their mathematical expressions) can be totally different in case (a) and case (b) because of the Lorentz force acting on the moving carriers.

Consider case (a) corresponding to $\mu_L < \mu_R$; then $i(E)$ defined in equation (11) assumes the following expression

$$i^{(a)}_{0n,1n}(E) = i_0\, 2\Re \begin{cases} \Big[G^R_{11} \Sigma^{R(\text{left})}_{11} - G^R_{11} \Sigma^{A(\text{left})}_{11} \\ \quad - i G^R_{11} \Gamma^{(\text{left})}_{11} G^A_{11} \Sigma^{A(\text{left})}_{11} \\ \quad - i G^R_{1M} \Gamma^{(\text{right})}_{MM} G^A_{M1} \Sigma^{A(\text{left})}_{11} \Big]_{nn} & \\ \qquad\qquad E < \mu_L < \mu_R & \\ \Big[- i G^R_{1M} \Gamma^{(\text{right})}_{MM} G^A_{M1} \Sigma^{A(\text{left})}_{11} \Big]_{nn} & \\ \qquad\qquad \mu_L < E < \mu_R & \\ 0 \qquad\qquad \mu_L < \mu_R < E. \end{cases} \tag{12}$$

The branch current $I_{0n,1n}$ of equation (10b) is obtained performing the integration of the spectral current on the energy variable. The integration extends from $E = -\infty$ to $E = \mu_R$ and is performed separately in the energy regions $E < \mu_L$ and $\mu_L < E < \mu_R$ adopting the corresponding appropriate expression for the spectral current reported in equation (12). The integral in the energy interval $[-\infty, \mu_L]$ is obviously restricted to the interval $[E_{min}, \mu_L]$, where E_{min} is the lowest eigenvalue of the electron system Hamiltonian.

Consider now case (b) corresponding to $\mu_R < \mu_L$; the spectral current $i(E)$ of equation (11) assumes the following expression

$$i^{(b)}_{0n,1n}(E) = i_0\, 2\Re \begin{cases} \Big[G^R_{11} \Sigma^{R(\text{left})}_{11} - G^R_{11} \Sigma^{A(\text{left})}_{11} \\ \quad - i G^R_{11} \Gamma^{(\text{left})}_{11} G^A_{11} \Sigma^{A(\text{left})}_{11} \\ \quad - i G^R_{1M} \Gamma^{(\text{right})}_{MM} G^A_{M1} \Sigma^{A(\text{left})}_{11} \Big]_{nn} & \\ \qquad\qquad E < \mu_R < \mu_L & \\ \Big[G^R_{11} \Sigma^{R(\text{left})}_{11} - G^R_{11} \Sigma^{A(\text{left})}_{11} \\ \quad - i G^R_{11} \Gamma^{(\text{left})}_{11} G^A_{11} \Sigma^{A(\text{left})}_{11} \Big]_{nn} & \\ \qquad\qquad \mu_R < E < \mu_L & \\ 0 \qquad\qquad \mu_R < \mu_L < E. \end{cases} \tag{13}$$

It can be noticed that the bottom (and top) expressions of equations (12) and (13) are coincident, while the intermediate expressions are different; the reason for this difference, and the role of magnetic fields in making them different, will be discussed in the next section.

We can simplify somewhat the formulas using the identities given in equations (3) and (4). We have

$$\begin{aligned} & G^R_{11} \Sigma^{R(\text{left})}_{11} - G^R_{11} \Sigma^{A(\text{left})}_{11} - i G^R_{11} \Gamma^{(\text{left})}_{11} G^A_{11} \Sigma^{A(\text{left})}_{11} \\ & \quad - i G^R_{1M} \Gamma^{(\text{right})}_{MM} G^A_{M1} \Sigma^{A(\text{left})}_{11} = \\ & G^R_{11} \Sigma^{R(\text{left})}_{11} - G^R_{11} \Sigma^{A(\text{left})}_{11} + (G^R_{11} - G^A_{11}) \Sigma^{A(\text{left})}_{11} \\ & = G^R_{11} \Sigma^{R(\text{left})}_{11} - G^A_{11} \Sigma^{A(\text{left})}_{11} . \end{aligned}$$

From the above expression we have

$$\begin{aligned} & G^R_{11} \Sigma^{R(\text{left})}_{11} - G^R_{11} \Sigma^{A(\text{left})}_{11} - i G^R_{11} \Gamma^{(\text{left})}_{11} G^A_{11} \Sigma^{A(\text{left})}_{11} = \\ & G^R_{11} \Sigma^{R(\text{left})}_{11} - G^A_{11} \Sigma^{A(\text{left})}_{11} + i G^R_{1M} \Gamma^{(\text{right})}_{MM} G^A_{M1} \Sigma^{A(\text{left})}_{11} \\ & = G^R_{11} \Sigma^{R(\text{left})}_{11} - G^A_{11} \Sigma^{A(\text{left})}_{11} + i G^R_{11} \Gamma^{(\text{right})}_{11} G^A_{11} \Sigma^{A(\text{left})}_{11} . \end{aligned}$$

We also notice that

$$\begin{aligned} \Re \Big[G^A_{11} \Sigma^{A(\text{left})}_{11} \Big]_{nn} & = \Re \Big[(G^A_{11} \Sigma^{A(\text{left})}_{11})^\dagger \Big]_{nn} \\ & = \Re \Big[\Sigma^{R(\text{left})}_{11} G^R_{11} \Big]_{nn} . \end{aligned}$$

By using the above relations, equation (12) can be recast in the form

$$i^{(a)}_{0n,1n}(E) = i_0\, 2\Re \begin{cases} \left[G^R_{11}\Sigma^{R(\text{left})}_{11} - \Sigma^{R(\text{left})}_{11}G^R_{11}\right]_{nn} \\ \qquad E < \mu_L < \mu_R \\ \left[-iG^R_{11}\Gamma^{(\text{right})}_{11}G^A_{11}\Sigma^{A(\text{left})}_{11}\right]_{nn} \\ \qquad \mu_L < E < \mu_R \\ 0 \qquad \mu_L < \mu_R < E. \end{cases} \tag{14}$$

Similarly equation (13), valid in the case $\mu_R < \mu_L$, takes the form

$$i^{(b)}_{0n,1n}(E) = i_0\, 2\Re \begin{cases} \left[G^R_{11}\Sigma^{R(\text{left})}_{11} - \Sigma^{R(\text{left})}_{11}G^R_{11}\right]_{nn} \\ \qquad E < \mu_R < \mu_L \\ \left[G^R_{11}\Sigma^{R(\text{left})}_{11} - \Sigma^{R(\text{left})}_{11}G^R_{11} \right. \\ \qquad \left. + iG^R_{11}\Gamma^{(\text{right})}_{11}G^A_{11}\Sigma^{A(\text{left})}_{11}\right]_{nn} \\ \qquad \mu_R < E < \mu_L \\ 0 \qquad \mu_R < \mu_L < E. \end{cases} \tag{15}$$

Equations (14) and (15) constitute the basic result for the theoretical imaging of longitudinal currents in the sample. These expressions are the most convenient both for analytic considerations and numerical simulations. We discuss now the transverse currents with similar procedures.

3.2 Expression of the transverse currents

The transverse current along a bond from site $1n$ to site $1\,n+1$ in steady state conditions is given by the expression

$$\begin{aligned} I_{1n,1\,n+1} &= \frac{2(-e)}{\hbar}\int \frac{dE}{2\pi}\, 2\Re\left[t_{1n,1\,n+1}G^<_{1\,n+1,1n}\right] \\ &= -i_0\int dE\, 2\Re\left[t_{1n,1\,n+1}G^<_{1\,n+1,1n}\right]. \end{aligned} \tag{16}$$

In the above equation, the lesser Green's function involves automatically matrix elements only among orbitals of Col. 1 of the central device, and there is no need of the preliminary elaborations performed in the previous subsection for the longitudinal current. In fact to proceed further we simply use the lesser Green's function projected on the sites of Col. 1, given by equation (9). The transverse branch current of equation (16) becomes

$$\begin{aligned} I_{1n,1\,n+1} &= -i_0\int dE\, 2\Re\left\{t_{1n,1\,n+1}\left[if_LG^R_{11}\Gamma^{(\text{left})}_{11}G^A_{11} \right.\right. \\ &\qquad \left.\left. + if_RG^R_{1M}\Gamma^{(\text{right})}_{MM}G^A_{M1}\right]_{n+1,n}\right\} \\ &= -i_0\int dE\, 2\Re\left\{t_{1n,1\,n+1}\left[if_LG^R_{11}\Gamma^{(\text{left})}_{11}G^A_{11} \right.\right. \\ &\qquad \left.\left. + if_RG^R_{11}\Gamma^{(\text{right})}_{11}G^A_{11}\right]_{n+1,n}\right\}. \end{aligned} \tag{17}$$

As before, we consider preliminarily the situation for zero temperature (and postpone the treatment of finite temperatures to Sect. 6). At the absolute zero temperature, the two Fermi distribution functions become step functions $f_L(E) = \Theta(\mu_L - E)$ and $f_R(E) = \Theta(\mu_R - E)$. Thus in the case $\mu_L < \mu_R$ the expression (17) takes the following form

$$I_{1n,1\,n+1} = \int i^{(a)}_{1n,1\,n+1}(E)\, dE \tag{18a}$$

where

$$i^{(a)}_{1n,1\,n+1}(E) = i_0\, 2\Re \begin{cases} t_{1n,1\,n+1}\left[-iG^R_{11}\Gamma^{(\text{left})}_{11}G^A_{11} \right. \\ \qquad \left. -iG^R_{11}\Gamma^{(\text{right})}_{11}G^A_{11}\right]_{n+1,n} \\ \qquad E < \mu_L < \mu_R \\ t_{1n,1\,n+1}\left[-iG^R_{11}\Gamma^{(\text{right})}_{11}G^A_{11}\right]_{n+1,n} \\ \qquad \mu_L < E < \mu_R \\ 0 \qquad \mu_L < \mu_R < E. \end{cases} \tag{18b}$$

In the opposite situation $\mu_R < \mu_L$ (case b), expression (17) takes the form

$$I_{1n,1\,n+1} = \int i^{(b)}_{1n,1\,n+1}(E)\, dE \tag{19a}$$

where

$$i^{(b)}_{1n,1\,n+1}(E) = i_0\, 2\Re \begin{cases} t_{1n,1\,n+1}\left[-iG^R_{11}\Gamma^{(\text{left})}_{11}G^A_{11} \right. \\ \qquad \left. -iG^R_{11}\Gamma^{(\text{right})}_{11}G^A_{11}\right]_{n+1,n} \\ \qquad E < \mu_R < \mu_L \\ t_{1n,1\,n+1}\left[-iG^R_{11}\Gamma^{(\text{left})}_{11}G^A_{11}\right]_{n+1,n} \\ \qquad \mu_R < E < \mu_L \\ 0 \qquad \mu_R < \mu_L < E. \end{cases} \tag{19b}$$

We can simplify somewhat the expression at the top of equations (18b) and (19b) using once more the identities described in equations (4). In particular we have

$$\left[-iG^R_{11}\Gamma^{(\mathrm{left})}_{11}G^A_{11} - iG^R_{11}\Gamma^{(\mathrm{right})}_{11}G^A_{11}\right]_{n+1,n} =$$

$$\left[G^R_{11} - G^A_{11}\right]_{n+1,n} = \left[G^R_{1\,n+1,1n} - G^A_{1\,n+1,1n}\right].$$

Equations (14, 15, 18) and (19) are the basic expressions for the theoretical imaging of current profiles in the longitudinal direction and in the transverse direction respectively. The results are reported for convenience in Table 1, which summarizes the current expressions, at zero temperature, for the theoretical imaging of current profiles in two-dimensional electron systems. The corresponding expressions at finite temperatures will be reported in Table 3.

4 Theoretical imaging of current profiles in time-reversal symmetric systems

The expressions deduced in Section 3, and summarized in Table 1, are the central result of this work for the calculation of the local currents through any branch. They hold for any electronic system, described by a Hamiltonian of type (1), regardless of the presence or not of time-reversal symmetry. However, much can be learned on the structure and physical meaning of the expressions elaborated so far considering the cases in which the electron Hamiltonian is invariant by time-reversal symmetry.

The first basic consideration is that, in the presence of time-reversal symmetry, it holds

$$I^{(a1)}_{0n,1n} = I^{(b1)}_{0n,1n} = I^{(a1)}_{1n,1\,n+1} = I^{(b1)}_{1n,1\,n+1} \equiv 0; \qquad (20)$$

any of the above four terms can be different from zero only in the absence of time-reversal symmetry.

Systems of spinless electrons are said to belong to the orthogonal or the unitary class of symmetry, if they are in the presence or in the absence of time-reversal symmetry, respectively. It is easy to show that the contributing terms (20) to the branch current vanish identically in the orthogonal class case. In fact when a system is invariant by time-reversal symmetry, we can assume that the basis functions are real and that the matrix elements of the Hamiltonian are real and symmetric; this entails that also the advanced and retarded Green's functions are symmetric (although not real, in general). In other words, the propagator from a given site i to any other site j and the propagator from site j to site i are equal: $G^R_{ji} \equiv G^R_{ij}$. This equality does not hold any more in the presence of magnetic fields. The trivial reason for this is the Lorentz force, automatically embodied in the Hamiltonian describing a system in the presence of magnetic fields.

We have thus in the presence of time-reversal symmetry the properties

$$t_{ij} = t^*_{ij}, \quad G^A_{ij} = G^A_{ji}, \quad G^R_{ij} = G^R_{ji}.$$

Table 1. Expressions, at zero temperature, for the theoretical imaging of the branch current profiles in two-dimensional systems. These expressions are valid both in the presence and in the absence of time-reversal symmetry. As discussed in the text, the terms with superscripts $(a1)$ and $(b1)$ describe persistent contributions to the currents, those with superscripts $(a2)$ and $(b2)$ describe transport contributions.

Longitudinal current for $\mu_L < \mu_R$

$$I_{0n,1n} = I^{(a1)}_{0n,1n} + I^{(a2)}_{0n,1n}$$

$$I^{(a1)}_{0n,1n} = i_0\int_{-\infty}^{\mu_L} dE\, 2\Re\left[G^R_{11}\Sigma^{R(\mathrm{left})}_{11} - \Sigma^{R(\mathrm{left})}_{11}G^R_{11}\right]_{nn}$$

$$I^{(a2)}_{0n,1n} = i_0\int_{\mu_L}^{\mu_R} dE\, 2\Re\left[-iG^R_{11}\Gamma^{(\mathrm{right})}_{11}G^R_{11}\Sigma^{A(\mathrm{left})}_{11}\right]_{nn}$$

Longitudinal current for $\mu_R < \mu_L$

$$I_{0n,1n} = I^{(b1)}_{0n,1n} + I^{(b2)}_{0n,1n}$$

$$I^{(b1)}_{0n,1n} = i_0\int_{-\infty}^{\mu_R} dE\, 2\Re\left[G^R_{11}\Sigma^{R(\mathrm{left})}_{11} - \Sigma^{R(\mathrm{left})}_{11}G^R_{11}\right]_{nn}$$

$$I^{(b2)}_{0n,1n} = i_0\int_{\mu_R}^{\mu_L} dE\, 2\Re\left[G^R_{11}\Sigma^{R(\mathrm{left})}_{11} - \Sigma^{R(\mathrm{left})}_{11}G^R_{11} + iG^R_{11}\Gamma^{(\mathrm{right})}_{11}G^R_{11}\Sigma^{(\mathrm{left})}_{11}\right]_{nn}$$

Transverse current for $\mu_L < \mu_R$

$$I_{1n,1\,n+1} = I^{(a1)}_{1n,1\,n+1} + I^{(a2)}_{1n,1\,n+1}$$

$$I^{(a1)}_{1n,1\,n+1} = i_0\int_{-\infty}^{\mu_L} dE\, 2\Re\left\{t_{1n,1\,n+1}\left[G^R_{1\,n+1,1n} - G^A_{1\,n+1,1n}\right]\right\}$$

$$I^{(a2)}_{1n,1\,n+1} = i_0\int_{\mu_L}^{\mu_R} dE\, 2\Re\left\{t_{1n,1\,n+1}\left[-iG^R_{11}\Gamma^{(\mathrm{right})}_{11}G^A_{11}\right]_{n+1,n}\right\}$$

Transverse current for $\mu_R < \mu_L$

$$I_{1n,1\,n+1} = I^{(b1)}_{1n,1\,n+1} + I^{(b2)}_{1n,1\,n+1}$$

$$I^{(b1)}_{1n,1\,n+1} = i_0\int_{-\infty}^{\mu_R} dE\, 2\Re\left\{t_{1n,1\,n+1}\left[G^R_{1\,n+1,1n} - G^A_{1\,n+1,1n}\right]\right\}$$

$$I^{(b2)}_{1n,1\,n+1} = i_0\int_{\mu_R}^{\mu_L} dE\, 2\Re\left\{t_{1n,1\,n+1}\left[-iG^R_{11}\Gamma^{(\mathrm{left})}_{11}G^A_{11}\right]_{n+1,n}\right\}$$

It follows

$$\Re[t_{ij}(G^R_{ji} - G^A_{ji})] = t_{ij}\Re[G^R_{ji} - G^{R*}_{ij}] = t_{ij}\Re[G^R_{ji} - G^{R*}_{ji}] \equiv 0.$$

If the suffix i stands for $1n$, and the suffix j stands for $1\,n+1$, it is seen that in the presence of time-reversal symmetry

$$\Re\, t_{1n,1n+1}\left[G^R_{1n+1,1n} - G^A_{1n+1,1n}\right] \equiv 0; \qquad (21a)$$

thus the last two of the relations (20) are demonstrated.

A similar demonstration shows that also the first two terms of equation (20) are identically zero. In fact, in the

Table 2. Expressions, at zero temperature, for the theoretical imaging of branch current profiles in two-dimensional electron systems with time-reversal symmetry. As discussed in the text, in the presence of time-reversal symmetry persistent currents vanish identically; the transport currents are described by the terms with superscripts $(a2)$ and $(b2)$, not vanishing in general.

Longitudinal current for $\mu_L < \mu_R$

$$I_{0n,1n} \equiv I^{(a2)}_{0n,1n} = i_0 \int_{\mu_L}^{\mu_R} dE\, 2\Re \left[-iG^R_{11} \Gamma^{(\mathrm{right})}_{11} G^R_{11} \Sigma^{A(\mathrm{left})}_{11} \right]_{nn}$$

Longitudinal current for $\mu_R < \mu_L$

$$I_{0n,1n} \equiv I^{(b2)}_{0n,1n} = i_0 \int_{\mu_R}^{\mu_L} dE\, 2\Re \left[+iG^R_{11} \Gamma^{(\mathrm{right})}_{11} G^R_{11} \Sigma^{(\mathrm{left})}_{11} \right]_{nn}$$

Transverse current for $\mu_L < \mu_R$

$$I_{1n,1\,n+1} \equiv I^{(a2)}_{1n,1\,n+1} = i_0 \int_{\mu_L}^{\mu_R} dE\, 2\Re \left\{ t_{1n,1\,n+1} \left[-iG^R_{11} \Gamma^{(\mathrm{right})}_{11} G^A_{11} \right]_{n+1,n} \right\}$$

Transverse current for $\mu_R < \mu_L$

$$I_{1n,1\,n+1} \equiv I^{(b2)}_{1n,1\,n+1} = i_0 \int_{\mu_R}^{\mu_L} dE\, 2\Re \left\{ t_{1n,1\,n+1} \left[-iG^R_{11} \Gamma^{(\mathrm{left})}_{11} G^A_{11} \right]_{n+1,n} \right\}$$

presence of time-reversal symmetry, Green's functions and self-energies are symmetric operators; thus it holds

$$\left[G^R_{11} \Sigma^{R(\mathrm{left})}_{11} - \Sigma^{R(\mathrm{left})}_{11} G^R_{11} \right]_{nn} = \sum_{n'} \left[G^R_{1n,1n'} \Sigma^{R(\mathrm{left})}_{1n',1n} - \Sigma^{R(\mathrm{left})}_{1n,1n'} G^R_{1n',1n} \right] = \sum_{n'} \left[G^R_{1n,1n'} \Sigma^{R(\mathrm{left})}_{1n',1n} - \Sigma^{R(\mathrm{left})}_{1n',1n} G^R_{1n,1n'} \right] \equiv 0. \quad (21b)$$

An alternative and perfectly equivalent demonstration could be done also starting from the identity

$$\Re \left[G^R_{11} \Sigma^{R(\mathrm{left})}_{11} - \Sigma^{R(\mathrm{left})}_{11} G^R_{11} \right]_{nn} \equiv \Re t_{0n,1n} [G^R_{1n,0n} - G^A_{1n,0n}]$$

and observing the vanishing of the second member of the above expression in the presence of time-reversal symmetry. This completes the demonstration of equation (20); the results are summarized in Table 2. From Table 2 it is seen by inspection that the interchange of the left and the right chemical potentials (for unchanged Hamiltonian) simply changes the sign of the currents.

The above considerations hold only for systems invariant by time-reversal symmetry. In broken time-reversal symmetry, and in the presence of sufficiently strong magnetic fields, the complete spatial separation of the left-propagating and right-propagating carriers may occur ("chiral regime") with peculiar properties on magneto-transport phenomena. As evident from Table 1, the interchange of the left and right chemical potentials can modify dramatically the distribution of microscopic currents flowing in the system.

5 Physics behind formulas: quantitative discerning of transport and persistent currents

In this section, we discuss the general results, elaborated in Section 3 and summarized in Table 1, in order to put in evidence the physical meaning behind formal expressions. Actually, a central achievement of our procedure is the clear quantitative description of transport and persistent currents in unitary class systems, as analytically highlighted in Section 5.1 and numerically illustrated in Section 5.2.

5.1 Transport and persistent currents within the Keldysh nonequilibrium formalism

For sake of simplicity let us consider the longitudinal current for instance in the case $\mu_L < \mu_R$ given in Table 1; the discussion for the transverse current, as well as for the case $\mu_R < \mu_L$, can be done along similar lines. The microscopic longitudinal currents for $\mu_L < \mu_R$ are given by the expression of Table 1

$$\begin{aligned} I_{0n,1n} &= I^{(a1)}_{0n,1n} + I^{(a2)}_{0n,1n} \\ &= i_0 \int_{-\infty}^{\mu_L} dE\, 2\Re \left[G^R_{11} \Sigma^{R(\mathrm{left})}_{11} - \Sigma^{R(\mathrm{left})}_{11} G^R_{11} \right]_{nn} \\ &\quad + i_0 \int_{\mu_L}^{\mu_R} dE\, 2\Re \left[-iG^R_{11} \Gamma^{(\mathrm{right})}_{11} G^A_{11} \Sigma^{A(\mathrm{left})}_{11} \right]_{nn}. \end{aligned} \quad (22)$$

Equation (22) holds for systems with or without time-reversal symmetry. The following considerations can be drawn from its analytic structure:

(i) as we have already noticed, when time-reversal symmetry is present, the Green's function and the self-energy operators are symmetric; thus according to equation (21b) it holds

$$\left[G^R_{11}(E) \Sigma^{R(\mathrm{left})}_{11}(E) - \Sigma^{R(\mathrm{left})}_{11}(E) G^R_{11}(E) \right]_{nn} \equiv 0$$

for any chosen energy E. This shows that the first term in the right hand side of equation (22) can be different from zero only in the absence of time-reversal symmetry;

(ii) the total current is obtained summing the contributions from all the chains crossing any arbitrary section of the device. This is done performing trace operation on the index n of the expression (22). Trace operation of a product of operators is invariant under cyclic permutation of operators, and then

$$\mathrm{Tr}\left[G^R_{11}(E)\Sigma^{R(\mathrm{left})}_{11}(E) - \Sigma^{R(\mathrm{left})}_{11}(E)G^R_{11}(E)\right] \equiv 0$$

i.e. in any energy interval the contribution to the total current originated from the first term in the right hand side of equation (22) is exactly zero. This holds independently from the presence of time-reversal symmetry in the system Hamiltonian. We have thus that the lead-to-lead total current (or applied current or measured current) flowing in the device is given by the relation

$$I = i_0 \int_{\mu_L}^{\mu_R} dE\, \mathrm{Tr}\left[G^R_{11}(E)\Gamma^{(\mathrm{right})}_{11}(E)G^A_{11}(E)\Gamma^{(\mathrm{left})}_{11}\right], \tag{23}$$

which recovers the Landauer-Büttiker two terminal scattering relation for charge transport [9], and remains valid also in cases where the leads are not invariant by space translations;

(iii) from expressions (22) and (23) it is evident that within the Keldysh tight-binding nonequilibrium formalism, imaging of currents as obtained from the branch current expression (22) requires an amount of work and computer memory comparable to what required for the more traditional calculation of the total currents by means of equation (23).

Consistently with the above remarks, we address for brevity the first term and the second term in equation (22) as *persistent* current component and *transport* current component, respectively; from now on we rewrite equation (22) (for the case $\mu_L < \mu_R$) in the self-explanatory form

$$I_{0n,1n} = I^{(\mathrm{persist})}_{0n,1n} + I^{(\mathrm{transp})}_{0n,1n} \tag{24a}$$

with

$$I^{(\mathrm{persist})}_{0n,1n} \equiv I^{(a1)}_{0n,1n} = i_0 \int_{-\infty}^{\mu_L} dE\, 2\Re\left[G^R_{11}\Sigma^{R(\mathrm{left})}_{11} - G^R_{11}\Sigma^{R(\mathrm{left})}_{11}\right]_{nn} \tag{24b}$$

and

$$I^{(\mathrm{transp})}_{0n,1n} \equiv I^{(a2)}_{0n,1n} = i_0 \int_{\mu_L}^{\mu_R} dE\, 2\Re\left[-iG^R_{11}\Gamma^{(\mathrm{right})}_{11}G^A_{11}\Sigma^{A(\mathrm{left})}_{11}\right]_{nn}. \tag{24c}$$

Quite similarly, all the terms with superscripts $(a1, b1)$ and $(a2, b2)$ appearing in Tables 1 and 2 can be interpreted as persistent and transport contributions to the currents, respectively. Regardless which is higher between the left and right chemical potentials μ_L and μ_R, from equations (24) and the similar ones in the tables, it is seen that "persistent currents" are supported by electronic states whose energies are lower than both chemical potentials, while "transport currents" are supported by electronic states whose energies are intermediate between the two chemical potentials. The analytic expressions in Table 1 also show that persistent currents (differently from transport currents) are unaffected by bias reversal of the device, obtained interchanging μ_L and μ_R; furthermore, by virtue of the general equations (21) persistent currents vanish identically in the presence of time-reversal symmetry. The exact quantitative expressions of persistent and transport components achieved in Section 3 has been made possible by the Keldysh theory of transport, which includes both currents carried from lead-to-lead scattering states, and diamagnetic currents non necessarily connected to the leads. The flow and role of persistent currents in unitary class systems can be inferred, for instance, from magnetization measurements [45] in two-dimensional electron gases subject to strong magnetic fields, or also from the predicted interference and magnetization phenomena in multichannel mesoscopic rings, threaded by steady or time-dependent magnetic fields [34,46].

5.2 Numerical simulations

In order to better clarify the matter discussed in the previous Sections, we evaluate numerically the expressions of Table 1 and provide the current flow in typical quantum wires in the presence and in the absence of magnetic fields perpendicular to the device. For the tight-binding representation of the two-dimensional electron gas [39–44], we adopt a square lattice discretization, with edge a, nearest neighbor interaction t, effective mass of the carriers m^*. Typical values adopted in the present simulation are $m^* = 0.068\ m_e$ (as in GaAs-AlGaAs heterostructures), $t = -90$ meV and then the lattice parameter $a = 2.5$ nm. The considered wire is arbitrarily long in the longitudinal direction; its transversal width $W = 300$ nm, corresponding to a total number of 121 chains, is chosen sufficiently larger than the magnetic length $\ell_B = (\hbar c/eB)^{1/2}$ (for fields of intensity $B = 5$ T, we have $\ell_B \approx 12$ nm, $\hbar\omega_c \approx 8.5$ meV). The translational symmetry in the longitudinal direction is artificially broken by a semicircular impenetrable island (of radius 75 nm). Impenetrable regions of the wire are safely mimicked by including in the Hamiltonian site energies $E_{mn} = E_0$ higher than the band width $4|t|$. In the numerical simulation below, the chemical potentials of the left and right reservoirs are $\mu_L = 14$ meV and $\mu_R = 15$ meV, or vice versa, both in the presence and in the absence of a perpendicular magnetic field of 5 T (along the positive z axis).

The (nearest-neighbor) tight-binding Hamiltonian, adopted to describe the device and the leads, is most suitable for the evaluation of self-energies and Green's functions by means of an appropriate mix of the powerful renormalization and decimation procedures [38–44]. The periodic parts of the open leads are formally eliminated

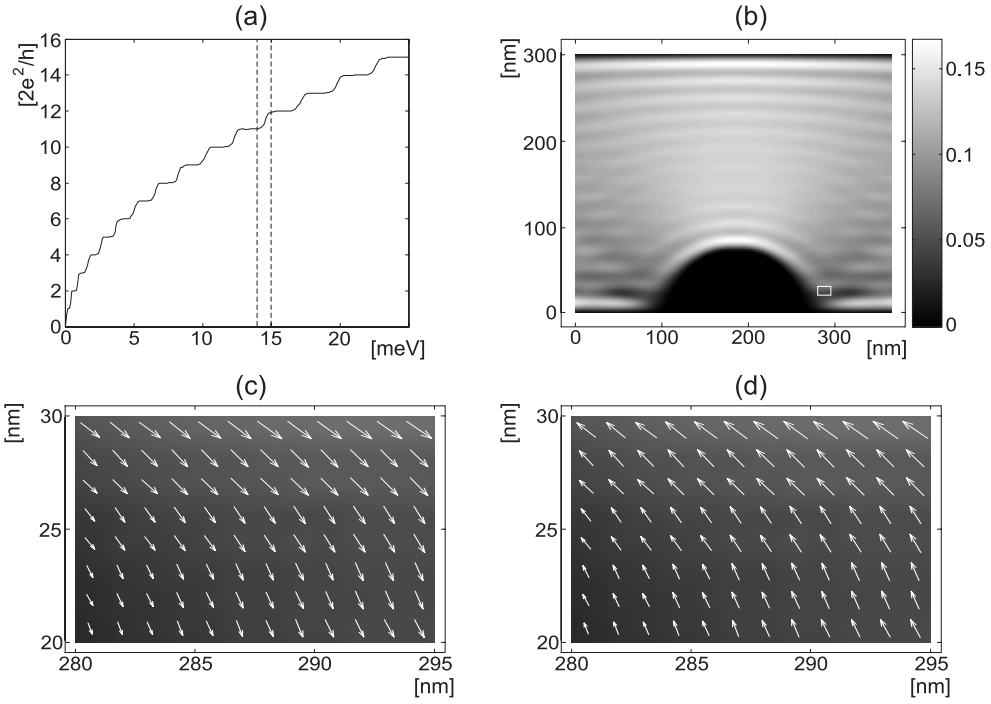

Fig. 2. (a) Differential conductance of the quantum wire described in the text, with an impenetrable island on the lower edge and in the absence of magnetic field. The dashed lines indicate the left and right chemical potentials $\mu_L = 14$ meV and $\mu_R = 15$ meV. (b) Spatial distribution of the transport current. The current flows all over the device and skips the impenetrable region. (c) Current profile in an enlarged region of the wire in the case $\mu_L = 14$ meV and $\mu_R = 15$ meV; the arrows indicate the intensity and the direction of the current. (d) Current profile in an enlarged region of the wire in the case $\mu_R = 14$ meV and $\mu_L = 15$ meV; the arrows indicate the intensity and the direction of the current. (c) and (d) coincide except for the directions of the arrows. The unit of current on the gray scale is I_0.

and replaced by the equivalent self-energies operators acting on the central device. The self-energies produced by the open leads are obtained with the renormalization technique, pursued until reaching the fixed-point [36] of the iterative procedure (a small number N_{iter} of steps corresponds to the processing of a total of $2^{N_{iter}}$ columns; twenty steps or so were definitely more than sufficient to give spectral currents with the accuracy of one part over million even in the presence of magnetic fields). Only in the central part of the devices, where translational symmetry is broken (by the superimposed impenetrable island, or any other irregularities) the reduction of the degrees of freedom is achieved eliminating a single column at a time. Green's functions and coupling operators are then obtained by handling the renormalized Hamiltonian (of rank N) on the preserved column; after storing whatever useful, this procedure is performed on every adjacent column in the region of interest of the device.

In Figure 2a, the differential conductance of the device in the absence of magnetic fields is reported. We notice the typical step-like shape, the precision of the step is partially affected by the presence of the obstacle. The dashed lines indicate the two chemical potentials μ_L and μ_R. Since time-reversal symmetry holds, the persistent current is zero, and transport and total microscopic currents coincide. The current distribution reported in Figure 2b is given by the integration of the transport spectral current between the two chemical potentials (see Tab. 2). The electron flow occurs throughout the bulk of the sample; interference fringes due to the obstacle and to the edges can be observed, and are signature of a coherent transport. Reversal of the potential bias simply entails the reversal of the current direction, without changing its microscopic distribution, as discussed in Section 4. This is illustrated by Figures 2c and 2d.

In Figure 3a, the differential conductance of the device in the presence of a perpendicular magnetic field of 5 T is reported. The differential conductance shows the typical plateaus of the integer quantum Hall effect. Each time a new Landau band is activated, the conductance increases by a quantum $2e^2/h$, as evident in Figure 3a. In the presence of magnetic fields, the persistent current is different from zero, since time-reversal symmetry is broken; furthermore, the distribution of transport current is deeply influenced by the sign of the potential bias. In Figures 3b and 3c the microscopic distribution of the persistent and transport currents are reported in the case $\mu_L = 14$ meV and $\mu_R = 15$ meV. Figure 3b shows that the persistent current flows in two spatially separated conductive channels bearing electrons in opposite directions at the opposite edges of the sample. Figure 3c shows that the transport current flows in the lower edge only and skips the obstacle without backscattering.

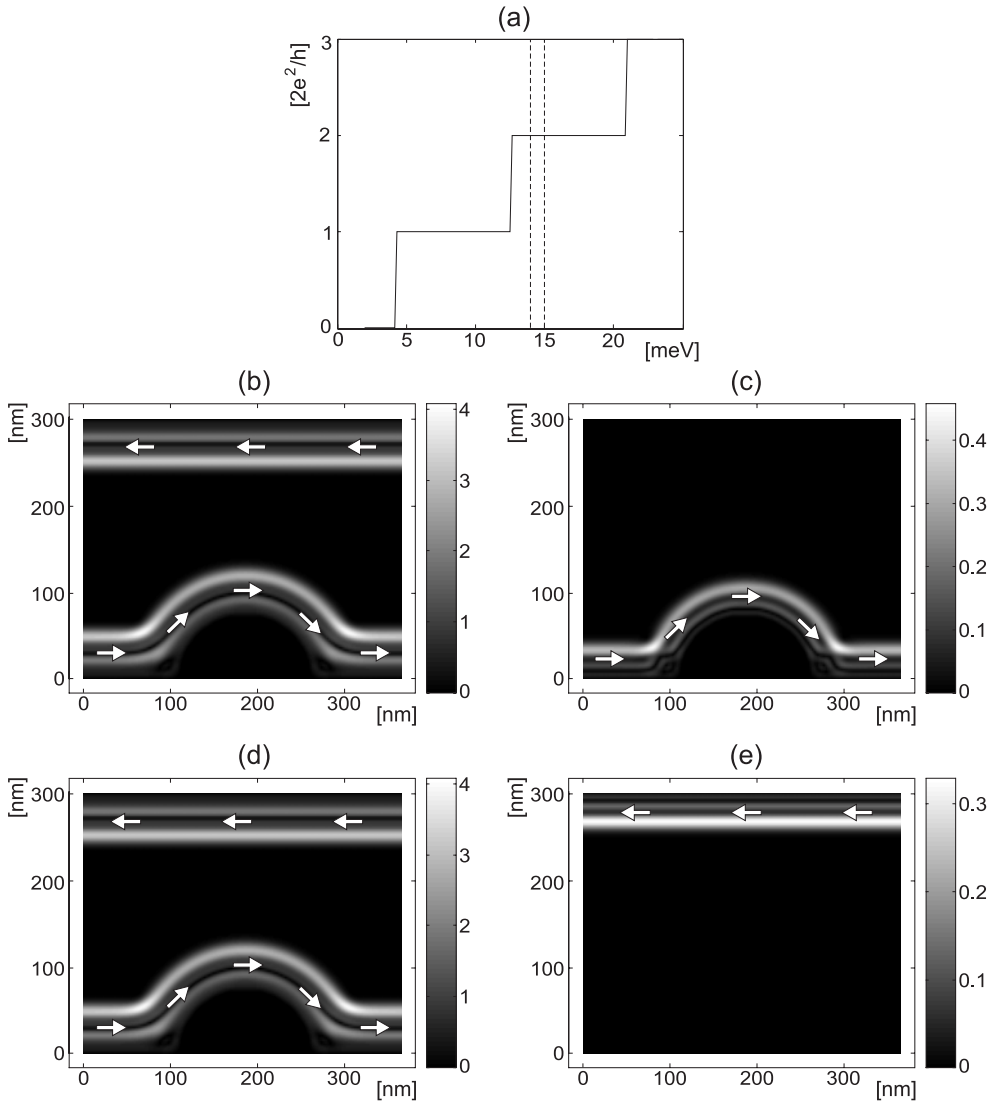

Fig. 3. (a) Differential conductance of the same sample of Figure 2, in the presence of a perpendicular magnetic field of 5 T. The dashed lines indicate the chosen left and right chemical potentials. (b) Spatial distribution of the persistent current in the case $\mu_L = 14$ meV and $\mu_R = 15$ meV. The arrows denote the current direction, and the unit on the gray scale is I_0. (c) Spatial distribution of the transport current in the case $\mu_L = 14$ meV and $\mu_R = 15$ meV. (d) Spatial distribution of the persistent current in the case $\mu_R = 14$ meV and $\mu_L = 15$ meV. This map and the map of case (b) are exactly the same. (e) Spatial distribution of the transport current in the case $\mu_R = 14$ meV and $\mu_L = 15$ meV. In this map, the current flows in the opposite direction and opposite edge of case (c).

This important peculiarity is due to the spatial chirality, i.e. the spatial separation between left moving and right moving carriers in strong magnetic fields, produced by the Lorentz force, automatically embodied in the formalism and the expressions of Table 1.

In the specific situation of Figures 3b–3c, it can be noticed that the transport current is much smaller than the persistent current, since the former is obtained by integrating the spectral contribution in the energy range between the two chemical potentials, while the latter is given by integrating the spectral contribution in the whole energy range below μ_L (see Tab. 1). As a consequence, persistent current can be locally much larger than transport currents; although these background currents may play a leading role in local magnetization and quantum interference phenomena [45,46], their net flow through any section of the sample is exactly zero. Vice versa, the calculated total transport current of Figure 3c is exactly quantized to $2I_0$, with a numerical accuracy better than one part per million (or even more if one wishes). Such a satisfactory numerical accuracy in the description of current profiles, even when dealing with arbitrary long wires in the presence of magnetic fields, is essentially linked the the extraordinary efficiency of the renormalization procedure in reaching the fixed-point renormalized Hamiltonian for the semi-infinite parts of the device [38].

The case $\mu_R = 14$ meV and $\mu_L = 15$ meV is considered in Figures 3d and 3e. In this situation the persistent

currents remain exactly the same as in Figure 3b, while the transport currents flow in the opposite direction on the opposite edge, again quantized to $2I_0$.

The analytic considerations of Section 5.1, together with the numerical calculation of this Section 5.2 (although restricted to the minimal models of Figs. 2, 3), give a feeling of the wealth of information and (accurate) technical simplicity of the theoretical imaging of currents, contained in the expressions of Table 1.

6 Current profiles at finite temperatures

The study of current profiles at finite temperatures can be obtained following step-by-step the same procedure adopted till now, and trivial replacement of zero temperature distribution functions of the leads with finite temperature distribution functions of the leads. The starting point for the deduction of e.g. the local longitudinal currents at $T \neq 0$ are again equations (10a, 10b) of Section 3.

In Section 3, we have seen that at zero temperature the spectral current entering equation (10a) is given by equation (11). At arbitrary finite temperatures $T \neq 0$, the spectral current entering equation (10a) is

$$i_{0n,1n} = i_0 f_L 2\Re \left[G^R_{11} \Sigma^{R(\text{left})}_{11} - G^R_{11} \Sigma^{A(\text{left})}_{11} - iG^R_{11} \Gamma^{(\text{left})}_{11} G^A_{11} \Sigma^{A(\text{left})}_{11} \right]_{nn} + i_0 f_R 2\Re \left[-iG^R_{1M} \Gamma^{(\text{right})}_{MM} G^A_{M1} \Sigma^{A(\text{left})}_{11} \right]_{nn}, \quad (25)$$

where $f_{L,R} = [\exp(E - \mu_{L,R})/k_B T + 1]^{-1}$. Starting from equation (25) and following step-by-step the procedure outlined in Section 3, we can easily work out all the expressions of current profiles at finite temperature. To give an example, the finite temperature version of equation (14) is just

$$i^{(a)}_{0n,1n}(E) = i_0 2\Re \left[G^R_{11} \Sigma^{R(\text{left})}_{11} - \Sigma^{R(\text{left})}_{11} G^R_{11} \right]_{nn} f_L(E) + i_0 2\Re \left[-iG^R_{11} \Gamma^{(\text{right})}_{11} G^A_{11} \Sigma^{A(\text{left})}_{11} \right]_{nn} [f_R(E) - f_L(E)].$$

There is no need to repeat here for $T \neq 0$ the straightforward procedure of Section 3. The results for $T \neq 0$ are reported in Table 3 which summarizes the contents of this work, also for what concerns the quantitative discerning of transport and persistent currents. Before closing, it is worthwhile to add that, in the presence of time-reversal symmetry, the analytic expressions of the current profiles at finite temperature (Tab. 3) exhibit universal features in line with those previously discussed at zero temperature (Tab. 1); this occurs by virtue of the general arguments discussed in Section 4. For the orthogonal class systems, in fact, equations (21) and Table 3 show that the persistent currents vanish identically, while the microscopic transport currents reverse their direction under bias reversal, without changing spatial distribution. These two properties of current distributions are no more true in broken time-reversal symmetry, where persistent currents are present and are unaffected by bias reversal, and transport currents change in general both direction and spatial distribution under bias reversal.

Table 3. Expressions, at arbitrary temperature, for the theoretical imaging of current profiles in systems with or without time-reversal symmetry.

Longitudinal current for $\mu_L < \mu_R$

$$I_{0n,1n} = I^{(\text{persist})}_{0n,1n} + I^{(\text{transp})}_{0n,1n}$$

$$I^{(\text{persist})}_{0n,1n} = i_0 \int dE f_L \, 2\Re \left[G^R_{11} \Sigma^{R(\text{left})}_{11} - \Sigma^{R(\text{left})}_{11} G^R_{11} \right]_{nn}$$

$$I^{(\text{transp})}_{0n,1n} = i_0 \int dE (f_R - f_L) \, 2\Re \left[-iG^R_{11} \Gamma^{(\text{right})}_{11} G^R_{11} \Sigma^{A(\text{left})}_{11} \right]_{nn}$$

Longitudinal current for $\mu_R < \mu_L$

$$I_{0n,1n} = I^{(\text{persist})}_{0n,1n} + I^{(\text{transp})}_{0n,1n}$$

$$I^{(\text{persist})}_{0n,1n} = i_0 \int dE f_R \, 2\Re \left[G^R_{11} \Sigma^{R(\text{left})}_{11} - \Sigma^{R(\text{left})}_{11} G^R_{11} \right]_{nn}$$

$$I^{(\text{transp})}_{0n,1n} = i_0 \int dE (f_L - f_R) 2\Re \left[G^R_{11} \Sigma^{R(\text{left})}_{11} - \Sigma^{R(\text{left})}_{11} G^R_{11} + iG^R_{11} \Gamma^{(\text{right})}_{11} G^R_{11} \Sigma^{(\text{left})}_{11} \right]_{nn}$$

Transverse current for $\mu_L < \mu_R$

$$I_{1n,1\,n+1} = I^{(\text{persist})}_{1n,1\,n+1} + I^{(\text{transp})}_{1n,1\,n+1}$$

$$I^{(\text{persist})}_{1n,1\,n+1} = i_0 \int dE f_L \, 2\Re \left\{ t_{1n,1\,n+1} \left[G^R_{1\,n+1,1n} - G^A_{1\,n+1,1n} \right] \right\}$$

$$I^{(\text{transp})}_{1n,1\,n+1} = i_0 \int dE (f_R - f_L) \, 2\Re \left\{ t_{1n,1\,n+1} \left[-iG^R_{11} \Gamma^{(\text{right})}_{11} G^A_{11} \right]_{n+1,n} \right\}$$

Transverse current for $\mu_R < \mu_L$

$$I_{1n,1\,n+1} = I^{(\text{persist})}_{1n,1\,n+1} + I^{(\text{transp})}_{1n,1\,n+1}$$

$$I^{(\text{persist})}_{1n,1\,n+1} = i_0 \int dE f_R \, 2\Re \left\{ t_{1n,1\,n+1} \left[G^R_{1\,n+1,1n} - G^A_{1\,n+1,1n} \right] \right\}$$

$$I^{(\text{transp})}_{1n,1\,n+1} = i_0 \int dE (f_L - f_R) \, 2\Re \left\{ t_{1n,1\,n+1} \left[-iG^R_{11} \Gamma^{(\text{left})}_{11} G^A_{11} \right]_{n+1,n} \right\}$$

7 Conclusions

In this paper we have focused on the theoretical imaging of microscopic currents in two-dimensional devices, both in the presence and in the absence of time-reversal symmetry. Our procedure not only pictures the spatial and energy distribution of carriers and currents, but also provides closed expressions for the persistent and lead-to-lead electron flow in mesoscopic devices. The concepts

and expressions, here provided in a systematic way, are of value to substantiate maps of edge and bulk conductive channels, persistent and transport charge currents in two-dimensional systems, also in the presence of impurities, disorder effects and boundaries, as shown by the simulations performed within the same background on quantum point contacts and random quantum wires [39,40]. Our formalism fully accounts also for the presence of magnetic fields, and embodies quantization and chirality conditions often encountered in magneto-transport experiments. Another nice feature of the present approach is that the ingredients necessary for computation of current profiles are restricted to propagators involving only the orbitals of single columns scanned through the device.

The basic tools exploited in the present procedure are the tight-binding representation of electronic states [7,8,36,38] and the Keldysh nonequilibrium Green's function theory [17,18,22–28]. The flexibility of the former and the generality of the latter, should make similar procedures of value also in dealing more sophisticated models of simulations, including for instance multi-orbital per site, spin-orbit coupling or other spin-dependent terms, successive neighbor interactions, models of many-body effects, different lattice topologies.

This work has been supported by Scuola Normale Superiore, and by National Enterprise for Nanoscience and Nanotechnology (NEST).

References

1. B.J. LeRoy, J. Phys.: Condens. Matter **15**, R1835 (2003)
2. M.A. Topinka, B.J. LeRoy, S.E.J. Shaw, R.M. Westervelt, R. Fleischmann, E.J. Heller, K.D. Maranowski, A.C. Gossard, Nature **410**, 183 (2001)
3. B.J. LeRoy, M.A. Topinka, A.C. Bleszynsky, R.M. Westervelt, S.E.J. Shaw, E.J. Heller, K.D. Maranowsky, A.C. Gossard, Appl. Surf. Science **210**, 134 (2003)
4. K.L. McCormick, M.T. Woodside, M. Huang, M. Wu, P.L. McEuen, C. Duruoz, J.S.Jr Harris, Phys. Rev. B **59**, 4654 (1999)
5. R. Crook, C.G. Smith, C.H.W. Barnes, M.Y. Simmons, D.A. Ritchie, J. Phys.: Condens. Matter **12**, L167 (2000)
6. C.W.J. Beenakker, H. Van Houten, in *Solid State Physics*, edited by H. Ehrenreich, D. Turnbull, Vol. **44** (Academic Press, 1991)
7. S. Datta, *Electronic Transport in Mesoscopic Systems* (Cambridge University Press, Cambridge, 1995)
8. D.K. Ferry, S.M. Goodnick, *Transport in Nanostructures* (Cambridge University Press, Cambridge, 1997)
9. M. Büttiker, Y. Imry, R. Landauer, S. Pinhas, Phys. Rev. B **31**, 6207 (1985)
10. H.U. Baranger, A. Douglas Stone, Phys. Rev. B **40**, 8169 (1989); H.U. Baranger, D.P. DiVincenzo, R.A. Jalabert, A. Douglas Stone, Phys. Rev. B **44**, 10637 (1991)
11. C.S. Lent, D.J. Kirkner, J. Appl. Phys. **67**, 6353 (1990)
12. T. Ando, Phys. Rev. B **44**, 8017 (1991)
13. P.A. Khomyakov, G. Brocks, V. Karpan, M. Zwierzycki, P.J. Kelly, Phys. Rev. B **72**, 035450 (2005)
14. F. Rossi, T. Kuhn, Rev. Mod. Phys. **74**, 895 (2002)
15. R. Lake, S. Datta, Phys. Rev. B **45**, 6670 (1992)
16. C. Caroli, R. Combescot, P. Nozieres, D. Saint-James, J. Phys. C.: Solid State Phys. **4**, 916 (1971); C. Caroli, R. Combescot, P. Nozieres, D. Saint-James, J. Phys. C.: Solid State Phys. **5**, 21 (1972)
17. L.P. Kadanoff, G. Baym, *Quantum Statistical Mechanics* (Benjamin, New York, 1962)
18. L.V. Keldysh, Zh. Éksp. Teor. Fiz. **47**, 1515 (1964) [Sov. Phys. JEPT **20**, 1018 (1965)]
19. A. Wacker, Phys. Rep. **357**, 1 (2002)
20. Y. Xue, S. Datta, M.A. Ratner, Chem. Phys. **281**, 151 (2002)
21. G.C. Liang, A.W. Ghosh, M. Paulsson, S. Datta, Phys. Rev. B **69**, 115302 (2004)
22. H. Haug, A.-P. Jauho, *Quantum Kinetics in Transport and Optics of Semiconductors* (Springer, Berlin, 2002)
23. M. Wagner, Phys. Rev. B **44**, 6104 (1991)
24. Y. Meir, N.S. Wingreen, Phys. Rev. Lett. **68**, 2512 (1992)
25. A.-P. Jauho, N.S. Wingreen, Y. Meir, Phys. Rev. B **50**, 5528 (1994)
26. A. Komnik, A.O. Gogolin, Phys. Rev. B **66**, 035407 (2002)
27. G. Chiappe, J.A. Vergás, J. Phys.: Cond. Matter **15**, 8805 (2002)
28. R. Lake, G. Klimeck, R.C. Bowen, D. Jovanovic, J. Appl. Phys. **81**, 7845 (1997)
29. P. Hyldgaard, S. Hershfield, J.H. Davies, J.W. Wilkins, Annals of Physics **236**, 1 (1994)
30. Zuo-Zi Chen, Rong Lü, Bang-fen Zhu, Phys. Rev. B **71**, 165324 (2005)
31. Z. Bihary, M.A. Ratner, Phys. Rev. B **72**, 115439 (2005)
32. L.G. Mourokh, N.J.M. Horing, A.Yu. Smirnov, Phys. Rev. B **66**, 085332 (2002)
33. E. Runge, H. Ehrenreich, Annals of Physics **219**, 55 (1992)
34. L. Arrachea, Eur. Phys. J. B **36**, 253 (2003)
35. F. Gagel, K. Maschke, Phys. Rev. B **52**, 2013 (1995)
36. T.N. Todorov, J. Phys.: Cond. Matt. **14**, 3049 (2002)
37. M.J. McLennan, Y. Lee, S. Datta, Phys. Rev. B **43**, 13846 (1990)
38. G. Grosso, S. Moroni, G. Pastori Parravicini, Phys. Rev. B **40**, 12328 (1989); G. Grosso, G. Pastori Parravicini, *Solid State Physics* (Academic Press, London, 2000)
39. A. Cresti, R. Farchioni, G. Grosso, G. Pastori Parravicini, Phys. Rev. B **68**, 075306 (2003)
40. A. Cresti, J. Appl. Phys. **98**, 013707 (2005)
41. M. Macucci, A. Galick, U. Ravaioli, Phys. Rev. B **52**, 5210 (1995)
42. M. Mendoza, P.A. Schulz, Phys. Rev. B **71**, 245303 (2005)
43. G. Metadilis, P. Bruno, Phys. Rev. B **72**, 235304 (2005)
44. F. Triozon, S. Roche, Eur. Phys. J. B **46**, 427 (2005)
45. D.R. Fauihaber, H.W. Jiang, Phys. Rev. B **72**, 233308 (2005)
46. P.A. Orellana, M. Pacheco, Phys. Rev. B **71**, 235330 (2005)